ISSN 1674-1056
http://cpb.iphy.ac.cn
http://iopscience.iop.org/cpb
中国物理 B
Chinese Physics
中国物理
Chinese Physics B

Site preferences of alloying transition metal elements in Ni-based superalloy: A first-principles study

Baokun Lu(路宝坤), Chong-Yu Wang(王崇愚), Zhihui Du(都志辉)

Citation: Chin. Phys. B . 2018, (9): 097102. **doi:** 10.1088/1674-1056/27/9/097102

Journal homepage: http://cpb.iphy.ac.cn; http://iopscience.iop.org/cpb

What follows is a list of articles you may be interested in

The effects of combining alloying elements on the elastic properties of *γ*-Ni in Ni-based superalloy: High-throughput first-principles calculations

Baokun Lu(路宝坤), Chongyu Wang(王崇愚)

Chin. Phys. B . 2018, 27(7): 077104. **doi:** 10.1088/1674-1056/27/7/077104

First principles study of the diffusional phenomena across the clean and Re-doped *γ*-Ni/*γ*'-Ni_3Al interface of Ni-based single crystal superalloy

Min Sun(孙敏), Chong-Yu Wang(王崇愚)

Chin. Phys. B . 2016, 25(6): 067104. **doi:** 10.1088/1674-1056/25/6/067104

Electronic structures and elastic properties of monolayer and bilayer transition metal dichalcogenidesMX_2 (*M*= Mo, W; *X*= O, S, Se, Te): A comparative first-principles study

Zeng Fan, Zhang Wei-Bing, Tang Bi-Yu

Chin. Phys. B . 2015, 24(9): 097103. **doi:** 10.1088/1674-1056/24/9/097103

Density functional calculations on 13-atom $Pd_{12}M$ (*M*=Sc-Ni) bimetallic clusters

Tang Chun-Mei, Chen Sheng-Wei, Zhu Wei-Hua, Tao Cheng-Jun, Zhang Ai-Mei, Gong Jiang-Feng, Zou Hua, Liu Ming-Yi, Zhu Feng

Chin. Phys. B . 2012, 21(11): 117101. **doi:** 10.1088/1674-1056/21/11/117101

Structural, elastic, phonon, and electronic properties of MnPd alloy

Wang Jun-Fei, Chen Wen-Zhou, Jiang Zhen-Yi, Zhang Xiao-Dong, Si Liang

Chin. Phys. B . 2012, 21(7): 077102. **doi:** 10.1088/1674-1056/21/7/077102

Site preferences of alloying transition metal elements in Ni-based superalloy: A first-principles study*

Baokun Lu(路宝坤)[1], Chong-Yu Wang(王崇愚)[1,†], and Zhihui Du(都志辉)[2]

[1] *Department of Physics, Tsinghua University, Beijing* 100084, *China*
[2] *Department of Computer Science and Technology, Tsinghua University, Beijing* 100084, *China*

(Received 19 June 2018; published online 28 August 2018)

Atomistic characterization of chemical element distribution is crucial to understanding the role of alloying elements for strengthening mechanism of superalloy. In the present work, the site preferences of two alloying elements *X*–*Y* in γ-Ni of Ni-based superalloy are systematically studied using first-principles calculations with and without spin-polarization. The doping elements *X* and *Y* are chosen from the 27 kinds of 3d, 4d, 5d group transition metals (Sc, Ti, V, Cr, Mn, Fe, Co, Cu, Zn, Y, Zr, Nb, Mo, Tc, Ru, Rh, Pd, Ag, Cd, Hf, Ta, W, Re, Os, Ir, Pt, Au) and Al. We find that the spin-polarized calculations for Re–Re, Re–Ru, Re–Cr, Ru–Cr show a strong chemical binding affinity between the solute elements and are more consistent with the experimental results. The binding energies of pairs between the 28 elements have an obvious periodicity and are closely related the electronic configuration of the elements. When the d-electrons of the element are close to the half full-shell state, two alloying elements possess attractive binding energies, reflecting the effect of the Hund's rule. The combinations of early transition metals (Sc, Ti, V, Y, Zr, Nb, Hf, Ta) have a repulsive interaction in γ-Ni. These results offer insights into the role of alloying elements for strengthening mechanism of superalloy.

Keywords: superalloy, transition metal, binding energy, cluster, first-principles calculations

PACS: 71.20.Be, 31.15.es, 71.15.Mb, 71.15.Nc **DOI:** 10.1088/1674-1056/27/9/097102

1. Introduction

Ni-base superalloys are unique high temperature materials, which display excellent high-temperature properties, such as strength, ductility, fracture toughness, fatigue resistance, creep resistance, and oxidation resistance.[1,2] Increasing demands for applications of such materials, mostly used in turbine blades of aircraft jet engines and land-based power generators, drive continued development of these alloys to perform in extreme conditions. The superalloys are characterized by cubical γ' precipitates (L12, ordered face-centered cubic (fcc), intermetallic compounds Ni_3Al) embedded in the γ matrix (disordered fcc, solid solution Ni).[1] In order to strengthen the single-crystal superalloys, nearly 10 elements are usually doped to improve the high temperature mechanical properties and their lifetime. Transition alloying elements Ti, Co, Cr, Nb, Mo, Ru, Ta, Hf, W, and Re are added to enhance the high-temperature properties. The elements Al and Ta are enriched in the γ' phase, while the elements Co, Cr, Mo, W, Re, and Ru are enriched in the γ matrix phase. Solid solution strengthening of the γ matrix is one key factor for improving the creep strength of Ni-base superalloys at high temperatures. Creep processes are largely controlled by the thermally activated motion of dislocations in the matrix phase, which requires dislocation climb at the γ/γ' interfaces. Elemental diffusion strongly influences the dislocation motion, thus it is important to consider the interaction of the solute elements. Among these alloying elements, Re remarkably improves the strength and creep resistance. The content of Re is considered as one of the characteristics in different-generation single-crystal superalloys, and in the newly developed fourth- and fifth-generation single-crystal superalloys.

However, no widely convinced mechanism has been conferred for the strengthening effect of Re until now. It was proposed that Re is present in the form of clusters in γ and acts as efficient obstacles for dislocation motion. Based on the results of one-dimensional atom probe (1DAP), Re clustering postulate was first suggested by Blavette *et al.*[3–5] Wanderka *et al.*[6] further used atom probe tomography (APT) to study the superalloy CMSX-4 and also concluded the formation of Re cluster. Rüsing *et al.*[7] used the more advanced three-dimensional atom probe (3DAP) and concluded that Re forms clusters with sizes of about 1 nm and mutual average distances of 20 nm. Mottura *et al.*[8] drew a contrary conclusion by using APT method, which took into account the detection efficiency and positional scatter of the atoms, and a purpose-built algorithm was used to analyze the atom probe datasets. They showed that the fluctuation in the ladder diagrams may be due to the random variation in the solute atoms and no solute clusters were detected in the Ni–Re binary alloys or the CMSX-4 single-crystal superalloys.[8,9] The experimental x-ray absorption fine structure (EXAFS) spectra were also compared to the simulated spectra, and it was shown that the experimental Ni–Re alloy does not display the double peaks in the spectra and

*Project supported by the National Key R&D Program of China (Grant Nos. 2017YFB0701501, 2017YFB0701502, and 2017YFB0701503).
†Corresponding author. E-mail: cywang@mail.tsinghua.edu.cn
© 2018 Chinese Physical Society and IOP Publishing Ltd

Re will not form clusters.[10]

In addition to these experimental studies, simulation methods were also used to check whether Re forms clusters or not in superalloys. The *ab initio* density functional theory simulations showed strong negative binding energies between Re–Re nearest neighbor pairs, and the repulsion energy for Re–Re pairs is rapidly reduced as the atoms are placed further apart.[10,11] Zhu *et al.*[12] used molecular dynamics (MD) simulations to calculate the binding energies of Re clusters in the Ni–Al–Re system and the results showed strong binding energies between Re atoms and indicated that Re tends to form clusters in the γ phase.

From a physical point of view, the co-segregation of Re with other alloying elements may be responsible for the strengthening effect of Re. The clusters built up by a couple of Re-solute atoms may play a major role in improving the creep strength of Re-containing superalloys.[13] Though not much information is available with the synergistic effects of Re with other alloying elements, some studies do give some indications of the synergy. Smith[14] studied a series of simple model alloys and showed that Cr strongly affects the partitioning of Re. And Re could not strengthen the superalloys without the addition of Cr. The following work of Chen *et al.*[15] showed similar behavior of the effect of Cr on Re and some bright contrast regions in the γ phase near the γ/γ' interface were found. Recently, Ge *et al.*[16] studied the distribution of Re in a second-generation single-crystal superalloy DD6 using high-angle annular dark-field scanning transmission electron microscope (HAADF–STEM) with the energy-dispersive spectroscopy (EDS) mapping. They suggested that Re and W may form clusters with sizes of about 1–2 nm in the γ phase close to the γ/γ' interface in crept superalloys, while no such clusters could be found near the γ/γ' interface before creep test. Co-segregation of Re with Co and Cr was observed at the tips of protrusions at the γ/γ' interface. As a result of coupling between the interfacial dislocation motion and the co-segregation of Re with Co and Cr, the creep rate in the steady creep regime was slowed down.[17] Yu *et al.*[18] used transmission electron microscopy and first-principles calculations to show that Re and Ru have a strong interaction, which results in the repartitioning of Re to the γ phase. Huang *et al.*[19] demonstrated that correlated element–element binding energies play a key role in the observed Ni retention-excesses at the γ-Ni/γ'-Ni_3Al interfaces during aging and evolution of the precipitates. In order to obtain deeper insight into the electronic mechanism of the element distribution, further theoretical calculations are needed to understand the interaction of Re element with other alloying elements at atomic-scale.

In the present work, via studying the binding energy of two doping elements, the site preferences of two alloying elements X–Y in γ-Ni of Ni-based superalloy are systematically studied using first-principles calculations with and without spin-polarization. The doping elements X and Y are chosen from the 27 kinds of 3d, 4d, 5d group transition metals (Sc, Ti, V, Cr, Mn, Fe, Co, Cu, Zn, Y, Zr, Nb, Mo, Tc, Ru, Rh, Pd, Ag, Cd, Hf, Ta, W, Re, Os, Ir, Pt, Au) and Al. We find that the spin-polarized calculations for Re–Re, Re–Ru, Re–Cr, Ru–Cr show a strong chemical binding affinity between the solute elements and more consistent with the experimental results. The binding energies of pairs between the 28 elements have an obvious periodicity and are closely related the electronic configurations of the elements. When d-electrons of an element is close to the half full-shell state, the doping element possesses an attractive binding energy, reflecting the effect of the Hund's rule. Meanwhile, the combination of early transition metals (Sc, Ti, V, Y, Zr, Nb, Hf, Ta) has a repulsive interaction in γ-Ni.

2. Methodology

2.1. Computational method

The first-principles calculations are based on electronic density-functional theory (DFT) and have been carried out using Vienna *ab initio* simulation package (VASP).[20–23] The electronic wave functions are expanded in plane waves with a kinetic-energy cutoff of 350 eV. For the DFT calculations, the projector augmented wave method[24] and the generalized gradient approximation of Perdew, Burke, and Ernzerhof[25] are used. A combination of conjugate gradient and quasi-Newton optimization methods is employed in this work to achieve faster geometry optimization due to high computational cost for calculating these large supercell systems. The volumes of all structures and the atomic arrangements are fully relaxed. The convergence criteria for the total energy and forces are chosen as 10^{-5} eV and 0.02 eV/Å, respectively. The Brillouin zone integrations are performed using Monkhorst–Pack[26] k-point meshes, a $5\times5\times5$ k-point mesh is used for the $3\times3\times3$ supercells, which is found to be sufficient to give fully converged results. We use the first-order Methfessel–Paxton[27] technique with the smearing parameter of 0.1 eV. The set of criteria achieves the generalized sufficient convergence condition. Spin-polarized and non-spin-polarized calculations are performed in the present study to take into account the effect of magnetism.

2.2. Computational model

Throughout this work, a 108 atom supercell model is used as shown in Fig. 1. There are 108 possible positions to replace an atom, and all positions are equivalent based on the crystal symmetry. When element X is doped at the corner site (0,0,0), there are a total of 107 possible sites for the second Y element to occupy. Taking into account the symmetry factors, there are

a total of 9 non-equivalent models. The difference between the 9 non-equivalent models is the distance between the two replacement atoms. The distance between the two doping elements at an i^{th} nearest neighbor (NN), the symmetry of the systems, the doping position of the second element Y, the number of equivalent models, and its weight are shown in Table 1. Doping elements X and Y are chosen from the 27 kinds of 3d, 4d, and 5d group transition metals (Sc, Ti, V, Cr, Mn, Fe, Co, Cu, Zn, Y, Zr, Nb, Mo, Tc, Ru, Rh, Pd, Ag, Cd, Hf, Ta, W, Re, Os, Ir, Pt, Au) and Al. X = Ni and Y = Ni correspond to the $Ni_{107}X$ and $Ni_{107}Y$ binary systems, respectively. There are a total of 784 possibilities, $Ni_{106}XY$ and $Ni_{106}YX$ are equivalent systems, so the number of non-equivalent systems is 406, including 378 ternary systems ($Ni_{106}XY$) and 28 binary systems ($Ni_{106}XX$).

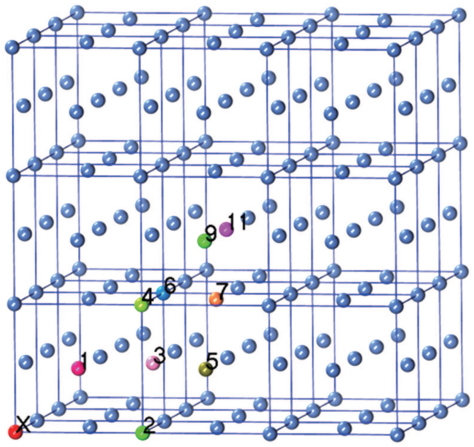


Fig. 1. (color online) The nine nearest neighbor pairs considered in 3×3×3 108 atoms supercell model.

Table 1. The nine nearest neighbor pairs are considered in 108 atoms model.

Atom number	i^{th} NN	Symmetry	Distance	Position	Number of equivalent models	Weight
1	1st NN	*Amm*2	$d_0\times\sqrt{1}$	(1/6,0,1/6)	12	0.11215
2	2nd NN	*P*4*mm*	$d_0\times\sqrt{2}$	(1/3,0,0)	6	0.05607
3	3rd NN	*Cm*	$d_0\times\sqrt{3}$	(1/3,1/6,1/6)	24	0.22430
4	4th NN	*Amm*2	$d_0\times\sqrt{4}$	(1/3,0,1/3)	12	0.11215
5	5th NN	*Pmm*2	$d_0\times\sqrt{5}$	(1/2,0,1/6)	12	0.11215
6	6th NN	*R*3*m*	$d_0\times\sqrt{6}$	(1/3,1/3,1/3)	8	0.07477
7	7th NN	*Pm*	$d_0\times\sqrt{7}$	(1/2,1/6,1/3)	24	0.22430
9	9th NN	*P*4/*mmm*	$d_0\times\sqrt{9}$	(1/2,0,1/2)	3	0.02804
11	11th NN	*P*4*mm*	$d_0\times\sqrt{11}$	(1/2,1/3,1/2)	6	0.05607

$d_0 = a_0/\sqrt{2}$, a_0 is lattice constants of Ni.

2.3. Binding energy

The binding energy between two doping defects at an i^{th} NN distance is calculated by subtracting the total energy of the system with the two doping defects at the i^{th} NN distance from the total energy of the system with the two doping defects at infinity.[19] It is given by

$$E^{i^{\text{th}}\text{NN}}_{\text{binding}} = E^{i^{\text{th}}\text{NN}}(\text{Ni}_{n-2}XY) - E(\text{Ni}_{n-2}XY)_{\text{infinity}}. \quad (1)$$

In a 3×3×3 supercell system, the 11th NN distance is far enough and the binding energy of the solute pairs is expected to reach 0 eV. The binding energy can be expressed as

$$E^{i^{\text{th}}\text{NN}}_{\text{binding}} = E^{i^{\text{th}}\text{NN}}(\text{Ni}_{106}XY) - E^{11^{\text{th}}\text{NN}}(\text{Ni}_{106}XY),$$
$$i = 1,2,3,4,5,6,7,9. \quad (2)$$

Also, if the supercell is large enough, the binding energy can be expressed as[11]

$$E^{i^{\text{th}}\text{NN}}_{\text{binding}} = [E^{i^{\text{th}}\text{NN}}(\text{Ni}_{n-2}XY) + E(\text{Ni}_n)] - [E(\text{Ni}_{n-1}X) + E(\text{Ni}_{n-1}Y)]. \quad (3)$$

In Eqs. (1) and (3), $E(\text{Ni}_{n-1}X)$ and $E(\text{Ni}_{n-1}Y)$ are the total energies of the supercell with a single X or Y atom, $E^{i^{\text{th}}\text{NN}}(\text{Ni}_{n-2}XY)$ is the total energy of the supercell with two doping atoms at an i^{th} NN distance, $E(\text{Ni}_n)$ is the total energy of a perfect supercell of Ni atoms and n is the total number of atoms in the system. Utilizing the above definition, a positive value of binding energy indicates a repulsive force between the two doping atoms, while a negative value indicates an attractive interaction. In this work, all of the binding energies are calculated by Eq. (3).

3. Result and discussion

In the previous work, Mottura *et al.*[11] concluded that magnetism is expected to have little effect on the binding energies of Re–Re, Ta–Ta, W–W pairs in the fcc-Ni lattice. To verify this conclusion, the binding energies between Re–Re, W–W, and Ta–Ta pairs are firstly calculated and the data are given in Table 2 and plotted in Fig. 2. The result based on non-spin-polarized calculations is consistent with that given by Mottura *et al.*[11] However, our results show that spin-polarized calculations and non-spin-polarized calculations will result in different conclusions for the Re–Re pairs. Therefore, the effect of magnetism on the binding energies of a X–Y nearest-neighbor pair is studied by comparing the spin-polarized and non-spin-

polarized calculations.

As shown in Table 1, the results show positive binding energies for Re–Re 1st NN and 2nd NN pairs by non-spin-polarized calculations, but negative binding energies by spin-polarized calculations, and the 2nd NN pair is energetically more stable. The 2nd NN rhenium pair is energetically stable at 0 K, suggesting that rhenium clusters would not form in the γ phase of single-crystal nickel-based superalloys. Therefore, it is expected that Re will approach a random distribution when alloyed in the γ phase with the concentration of 1.0–2.0 at.% typically used in these materials. Meanwhile, the results of W–W pairs and Ta–Ta pairs are almost the same in both spin-polarized and no-spin-polarized calculations. The repulsion energies observed for the Ta–Ta and W–W nearest neighbor pairs are rapidly reduced as the atoms are placed further apart, suggesting that the interactions between these solute atoms are strongly localized. It is possible to form short-range ordered structures and a Re–Re periodic chain along the ⟨100⟩ direction. Luo *et al.*[28] reported that heavy-atom columns align in the ⟨100⟩ and ⟨110⟩ directions and form heavy-atom stripes of about 1–2 nm in length. Heavy-atom ordering resembles the results reported by Maisel *et al.*,[29] which suggested that Re prefers to align in the ⟨420⟩ direction in the form of Ni_4Re. The Ni_4Re compound was shown to be stable by quantum mechanical high-throughput calculations at 0 K. Owing to the high diffusion activation energy of the heavy atoms and the stronger bonding strength of the refractory element with Ni, this short-range ordering will help to improve the mechanical performance.

Table 2. The binding energies (in eV) between Re–Re, W–W, and Ta–Ta pairs at different distances in single-crystal nickel-based superalloys.

	Re–Re			W–W			Ta–Ta		
i^{th} NN	non-spin	spin	non-spin[11]	non-spin	spin	non-spin[11]	non-spin	spin	non-spin[11]
1st NN	0.434	–0.190	0.425	0.615	0.529	0.598	0.685	0.323	0.679
2nd NN	0.067	–0.260	0.095	0.007	–0.197	0.013	–0.069	–0.191	–0.064
3rd NN	0.034	–0.130	0.046	0.040	–0.066	0.029	0.009	–0.076	0.010
4th NN	0.088	–0.052	0.109	0.075	–0.013	0.067	0.023	–0.004	0.030
5th NN	–0.011	–0.155	0.012	–0.015	–0.089	0.002	–0.047	–0.101	–0.042
6th NN	–0.005	–0.133	0.015	0.005	–0.014	0.011	–0.004	–0.036	0.003
7th NN	0.002	–0.041	–	0.005	–0.017	–	–0.008	–0.035	–
9th NN	–0.033	–0.129	–	–0.087	–0.114	–	–0.105	–0.142	–
11th NN	–0.001	–0.077	–	0.006	–0.020	–	–0.005	–0.037	–

Note: the formula for calculating the binding energy in Ref. [11] has a minus sign compared with the formula used in this paper.

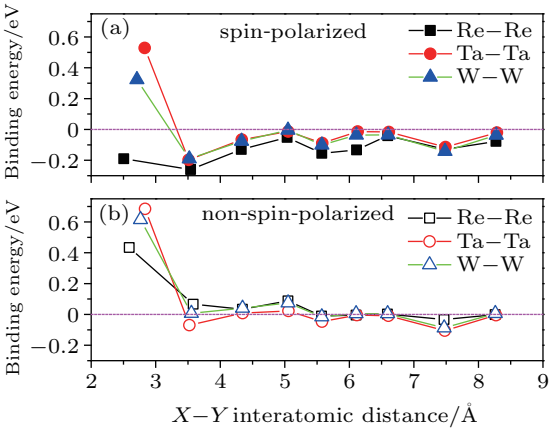


Fig. 2. (color online) The binding energies between Re–Re, W–W, and Ta–Ta pairs in a 3×3×3 fcc Ni supercell containing 108 atoms as a function of *X*–*X* separate distance: (a) spin-polarized calculations, (b) non-spin-polarized calculations.

The binding energies between *X*(Re, Ru)–*Y*(Re, W, Ta, Ru, Mo, Co, Cr, Al) pairs in $Ni_{106}XY$ system vs. *X*–*Y* separate distance are shown in Fig. 3. The binding energies essentially decay to zero when the distances between *X*–*Y* pairs increase. The interactions are only significant through the 3rd NN, which is not surprising as in a metallic alloy, the charges on the ion cores are screened strongly by the conduction free electrons.

We next discuss the effect of magnetism on the binding energies of an *X*–*Y* 1st NN pair by comparing the spin-polarized and non-spin-polarized calculations. The results are plotted in Fig. 4. It is shown that the binding energy strongly depends on the spin polarization. For example, under the spin-polarized calculations, the pairs of Re–Re, Re–Cr, Ru–Cr, Re–Ru, Ru–Mo, Ru–W, Re–Mo, and Mo–Cr at 1st NN have big attractive binding energies; while the pairs of Co–Cr, Co–Ru, Co–Mo, Co–W, Co–Re at 1st NN have a weak chemical repulsive tendency. The results of the non-spin polarization calculation are opposite to those of the spin polarization calculation. Under non-spin polarization conditions, most of pairs have big repulsive binding energies and are strongly repulsive in the first neighbor. Short-range order does not form, and it is randomly distributed over long-range. It is worth noted the results of Re–Cr, Ru–Cr, W–Cr, Ta–Cr, Re–Al, W–Al, Ta–Al, and Ru–Al with spin polarization are consistent with the experimental and calculation results reported by Huang *et al.*[19] The result of Re–Ru with spin polarization is consistent

with the previous calculation result and experimental results reported by our research group.[18] Based on the existing experimental results, we believe that the results of spin polarized calcuation are more convincing. Therefore the following discussion are mainly based on the results of spin polarized calcuation, meanwhile the data of nonspin polarized calcuation are given to understand the magnetic effect.

The detailed binding energies between *X* (Re, W, Ta, Ru, Mo, Co, Cr, Al) and *Y* (Re, W, Ta, Ru, Mo, Co, Cr, Al) pairs with 1st NN, 2nd NN, and 11th NN distances are listed in Table 3. In the spin-polarized calculations, for the binding energies of pairs of Al–*X*, Ta–*X*, and W–*X*, almost all the solute elements exhibit alternating positive and negative binding energies from the 1st to 2nd NN sites, which indicates that all refractory elements are substituting on the Al-sublattice and form an L12 ordered structure with Ni, except for Co. The pairs of Re–Ru, Re–Cr, Ru–Cr, Re–Re, Mo–Cr, Re–Mo, and Ru–Mo have attractive binding energies at 1st and 2nd NN distances. The results show that Re–Re, Re–Cr, Mo–Cr, and Re–Mo at 2nd NN are more stable, Re–Ru and Ru–Cr at 1st NN are more stable, consistent with the previous experimental and calculation results.[18,19] The binding energies of Co-*X* pairs are close to 0, indicating that cobalt and other elements interact relatively weakly. We believe that cobalt and other elements do not have preference of occupancy and are randomly distributed. From the above analysis of the binding energies, the metals can be divided into three classes: (i) Al, Ta, and W exhibit repulsive binding energies with second elements at the 1st NN distance, but they have attractive binding energies with the second element at the 2nd NN distance; (ii) Re, Mo, Cr, and Ru have an affinity with each other and attractive binding energies at 1st NN and 2nd NN distances; and (iii) Co interacts with other elements relatively weakly.

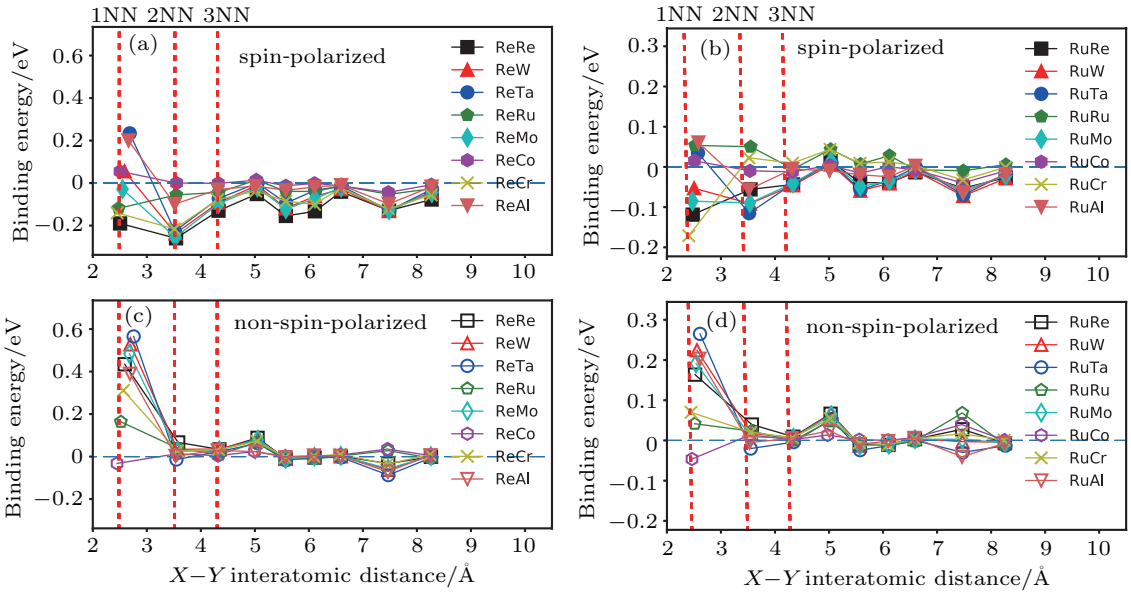


Fig. 3. The binding energies between *X*(Re, Ru)–*Y*(Re, W, Ta, Ru, Mo, Co, Cr, Al) pairs in $Ni_{106}XY$ system vs. *X*–*Y* separate distance: (a), (b) spin-polarized calculation; (c), (d) non-spin-polarized calculation. Ranges from the 1st NN to 3rd NN distances of pure Ni are indicated by the dashed vertical lines.

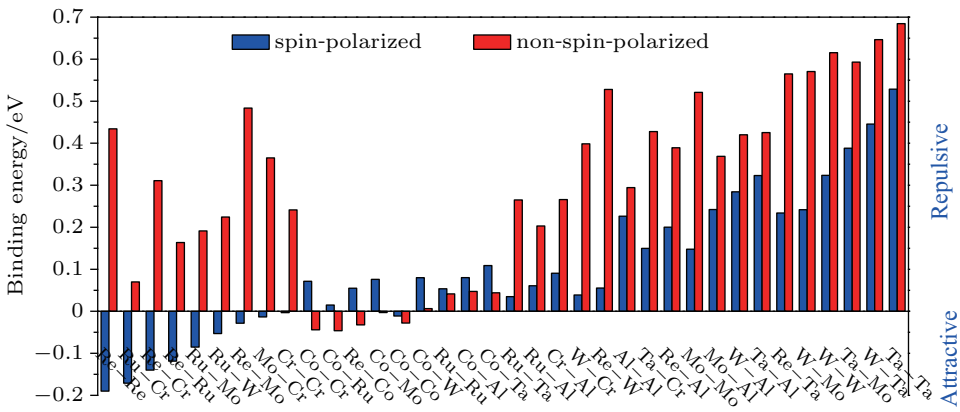


Fig. 4. The binding energies between *X*(Re, W, Ta, Ru, Mo, Co, Cr, Al)–*Y*(Re, W, Ta, Ru, Mo, Co, Cr, Al) pairs in $Ni_{106}XY$ system at 1st NN distance. The blue histogram represents the result of spin-polarized calculation, and the red histogram represents the result of non-spin-polarized calculation.

Table 3. The binding energies (in eV) between X(Re, W, Ta, Ru, Mo, Co, Cr, Al)–Y(Re, W, Ta, Ru, Mo, Co, Cr, Al) pairs in $Ni_{106}XY$ system at 1st NN, 2nd NN, and 11th NN distances.

X–Y system	Spin polarized calculation				Non-spin polarized calculation			
	1st NN	2nd NN	11th NN	site preference	1st NN	2nd NN	11th NN	site preference
Re–Ru	–0.119, –0.15[18]	–0.056, –0.10[18]	–0.027	1st NN	0.164	0.039	–0.007	repulsive random
Ru–Cr	–0.171, –0.211[19]	0.023, –0.172[19]	–0.001	1st NN	0.070	0.020	0.001	repulsive random
Re–Re	–0.190	–0.260	–0.077	2nd NN, 1st NN	0.434	0.067	–0.001	repulsive
Re–Cr	–0.140, –0.242[19]	–0.216, –0.154[19]	–0.056	2nd NN, 1st NN	0.311	0.027	0.009	repulsive random
Re–Mo	–0.028	–0.255	–0.046	2nd NN	0.484	0.024	0.002	repulsive random
Mo–Cr	–0.013	–0.203	–0.047	2nd NN	0.365	0.018	0.007	repulsive
Ru–Ta	0.035	–0.115	–0.017	2nd NN	0.265	–0.020	–0.013	repulsive random
Ru–Mo	–0.085	–0.090	–0.022	random	0.191	0.009	–0.006	repulsive
Ru–W	–0.053	–0.091	–0.028	random	0.224	0.017	–0.004	repulsive
Co–Cr	0.071	–0.024	–0.011	random	–0.044	–0.003	–0.001	random
Co–Ru	0.015	–0.010	–0.010	random	–0.046	0.013	0.001	random
Co–Re	0.055	0.000	–0.008	random	–0.032	0.013	0.005	random
Co–Mo	0.076	–0.002	–0.005	random	–0.003	0.010	0.003	random
Co–Co	–0.011	–0.015	–0.008	random	–0.028	0.002	0.003	random
Co–W	0.080	–0.003	–0.014	random	0.006	0.011	0.002	random
Co–Al	0.080	–0.010	–0.008	random	0.047	0.001	0.001	random
Co–Ta	0.109	–0.005	–0.009	random	0.044	0.003	–0.006	random
Ru–Ru	0.054	0.050	0.006	random	0.042	0.023	–0.010	random
Al–Al	0.226	–0.027	–0.006	random	0.294	0.023	–0.001	repulsive
Cr–Cr	–0.003	–0.091	–0.024	2nd NN	0.241	0.002	0.011	repulsive
Ru–Al	0.061, 0.372[19]	–0.056, –0.134[19]	–0.018	2nd NN	0.203	–0.005	–0.007	repulsive
Cr–Al	0.091	–0.069	–0.019	2nd NN	0.266	0.013	–0.001	repulsive
Re–Al	0.200, 0.281[19]	–0.099, –0.110[19]	–0.017	2nd NN	0.389	0.003	0.006	repulsive
Mo–Al	0.242	–0.080	–0.010	2nd NN	0.369	0.008	0.004	repulsive
W–Al	0.284, 0.194[19]	–0.086, –0.152[19]	–0.013	2nd NN	0.420	0.008	0.006	repulsive
Ta–Al	0.323, 0.156[19]	–0.074, –0.271[19]	–0.013	2nd NN	0.425	0.003	0.002	repulsive
W–Cr	0.039, 0.184[19]	–0.203, –0.186[19]	–0.043	2nd NN	0.399	0.023	0.005	repulsive
Re–W	0.055	–0.237	–0.040	2nd NN	0.528	0.034	0.005	repulsive
Ta–Cr	0.150, 0.292[19]	–0.184, –0.114[19]	–0.035	2nd NN	0.428	0.013	0.001	repulsive
Mo–Mo	0.148	–0.226	–0.026	2nd NN	0.521	–0.004	0.003	repulsive
Re–Ta	0.234	–0.226	–0.029	2nd NN	0.565	–0.014	–0.005	Repulsive
W–Mo	0.242	–0.208	–0.031	2nd NN	0.571	0.000	0.007	repulsive
W–W	0.323	–0.191	–0.037	2nd NN	0.615	0.007	0.006	repulsive
Ta–Mo	0.388	–0.192	–0.020	2nd NN	0.593	–0.037	–0.004	2nd NN
W–Ta	0.446	–0.192	–0.026	2nd NN	0.647	–0.033	0.000	2nd NN
Ta–Ta	0.529	–0.197	–0.020	2nd NN	0.685	–0.069	–0.005	2nd NN

Figure 5 shows the binding energies between Re and the other 28 elements. It is not difficult to find that the binding energy has an obvious periodicity, and different groups show different rules. In the spin-polarized calculations (see Fig. 5(a)), the 1st NN binding energy of Re–X exhibits a V-shaped curve, the lowest binding energy is located at half-full $d = 5$ and the value at the valley is less than 0. We believe that Re and other elements almost all have the 1st NN repulsive and 2nd NN attracting interaction energies, except that the pairs of Re–Re, Re–Cr, Re–Tc, Re–Ru, and Re–Os are attractive both at the 1st NN and 2nd NN. The binding energise of Re–Ru and Re–Os at 1st NN are lower than those at 2nd NN. It is possible to have short-range ordered structures in the ⟨110⟩ and ⟨100⟩ directions. Forming a Re-X periodic chain along the ⟨110⟩ direction may reflect the strengthening effect of Re. On the other hand, in the non-spin polarized calculation shown in Fig. 5(b), the 1st NN binding energy also exhibits a V-shaped curve, the lowest binding energy is located at $d = 7$ and the value at the valley is greater than 0, except for element Co. The binding energies at the second nearest neighbor are almost greater than 0, except that some early transiton metal elements (Sc, Ti, Y, Zr, Hf) at the 2nd NN have a weak attraction. The binding energies of Re–Co at the 1st NN and 2nd NN distances all approach 0, indicating that there is a random distribution between Re and Co.

In order to systematically study the interactions between elements in the periodic table and to explore the rules from the data, we calculate the binding energies between combinations of the 28 elements. The binding energies of X–Y pairs in $Ni_{106}XY$ system at 1st NN by spin polarized calculation and non-spin polarized calculation are shown in Figs. 6 and 7, respectively.

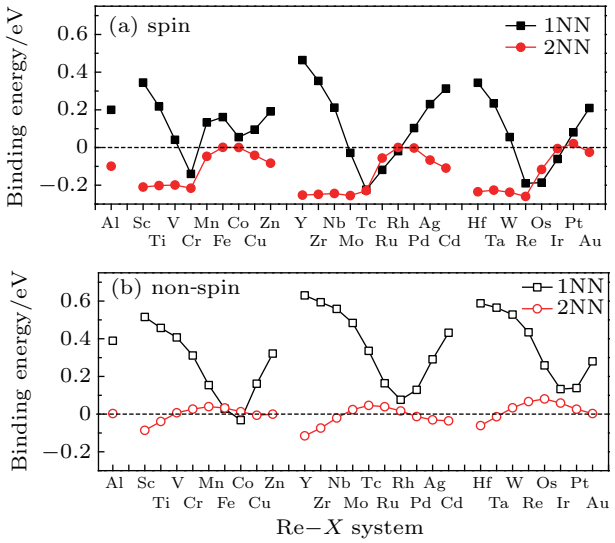


Fig. 5. The binding energies calculated with spinpolarization (a) and without spinpolarization (b) between X(Re)–Y(3d, 4d, 5d transition metal and Al) pairs in $Ni_{106}XY$ system at 1st and 2nd distances.

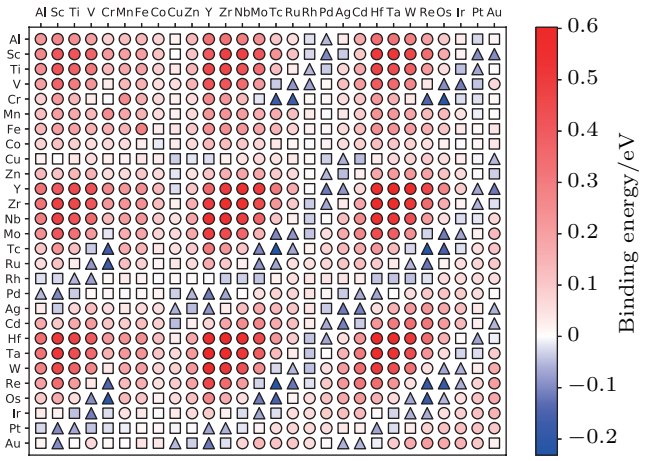


Fig. 6. The binding energies between X(3d, 4d, 5d transition metals and Al)–Y(3d, 4d, 5d transition metals and Al) pairs in $Ni_{106}XY$ system at 1st NN distance by spin polarized calculation.

In Figs. 6 and 7, the circle represents the positive binding energy, the triangle represents the negative binding energy, the box represents the binding energy close to zero. The deeper red color represents the greater binding energy, the darker blue color represents the more negative binding energy, the lighter color indicates that the binding energy is closer to zero. From Fig. 6, it can be found that the binding energies between the two elements have an obvious periodicity. The binding energy is closely related the electronic configuration of the elements. The behaviors of different elemental periods are not the same, the properties of 4d and 5d group elements are similar. For the early transition elements (Sc, Ti, V, Y, Zr, Nb, Hf, Ta), the sum of the d-electrons of the two element combinations is less than 6 and it exhibits repulsive effects. From the map, it is found that the triangular area forms a band, especially when the d electronic shell is fully filled ($X_d + Y_d = 9$, 10, 11), such as Re+Cr, Re+Re, Re+Ru, Ru+Cr, etc. Its magnitude will decrease rapidly with decreasing overlap of the d shells of the adjacent atoms. Its magnitude will therefore be smallest for those elements with $X_d + Y_d$ nearly fully filled: (i) $X_d + Y_d = 2$, 3, 4, 5, 6, 7, 8, repulsive binding energies for combinations of early transition metals; (ii) $X_d + Y_d = 9$, 10, 11, attractive binding energies when the d-electrons of the element close to half full-shell state possess attractive binding energies. These results reflect the effect of the Hund's rule.

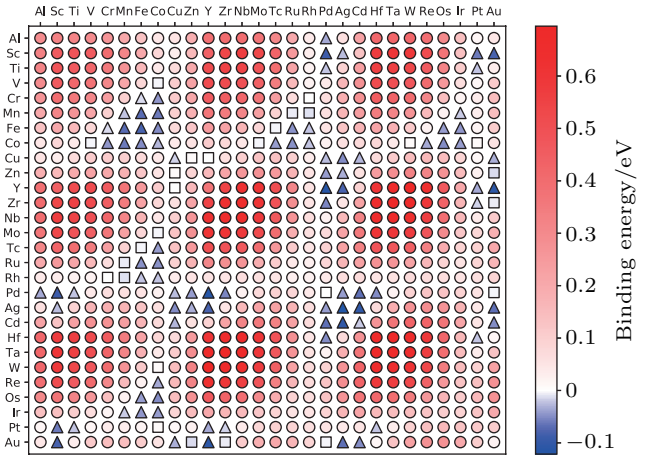


Fig. 7. The binding energies between X(3d, 4d, 5d transition metals and Al)–Y(3d, 4d, 5d transition metals and Al) pairs in $Ni_{106}XY$ system at 1st NN distance by non-spin polarized calculation.

This law may be related to the spin coupling between the incomplete d shells and the conduction electrons which leads to a tendency for a ferromagnetic alignment of the d electrons. Specific deep-level physics mechanism will be in-depth studied in future research. Additionally, further work studying the effects of alloy elements from electronic structure will always be of great importance.

4. Summary

The site preferences of two alloying elements X–Y in γ-Ni of Ni-based superalloy are systematically studied using first-principles calculations with and without spin-polarization. The doping elements X and Y are chosen from the 27 kinds of 3d, 4d, 5d group transition metals (Sc, Ti, V, Cr, Mn, Fe, Co, Cu, Zn, Y, Zr, Nb, Mo, Tc, Ru, Rh, Pd, Ag, Cd, Hf, Ta, W, Re, Os, Ir, Pt, Au) and Al. We find that the spin-polarized calculations for Re–Re, Re–Ru, Re–Cr, Ru–Cr show a strong chemical binding affinity between the solute elements and more consistent with the experimental results. The binding energies of pairs between the 28 elements have an obvious periodicity and are closely related the electronic configuration of the elements. When the d-electrons of the element is close to the half full-shell state, two alloying elements possess attractive binding energies, this result reflects the effect of the Hund's rule. The combination of early transition metals (Sc, Ti, V, Y, Zr, Nb, Hf, Ta) have a repulsive interaction in γ-Ni. These results offer insights into the role of alloying elements in strengthening mechanism of superalloy.

Acknowledgment

Simulations were performed using the Explorer 100 cluster system at the Tsinghua National Laboratory for Information Science and Technology, Beijing, China. Thanks to Sunway TaihuLight on National Supercomputing Center in Wuxi for supporting this research.

References

[1] Reed R C 2006 *The Superalloys: Fundamentals and Applications* (Cambridge: Cambridge University Press)
[2] Pollock T M and Tin S 2006 *J. Propulsion Power* **22** 361
[3] Blavette D, Caron P and Khan T 1986 *Scr. Metall.* **20** 1395
[4] Blavette D, Caron P and Khan T 1988 *Sixth Int. Symp. Superalloys-Superalloys* **1988** 305
[5] Blavette D, Cadel E, Pareige C, Deconihout B and Caron P 2007 *Microscopy Microanalysis* **13** 464
[6] Wanderka N and Glatzel U 1995 *Mater. Sci. & Eng. A (Structural Mater.: Properties Microstruct. Process.)* **A203** 69
[7] Rüsing J, Wanderka N, Czubayko U, Naundorf V, Mukherji D and Rösler J 2002 *Scr. Mater.* **46** 235
[8] Mottura A, Miller M K and Reed R C 2008 *The 11th International Symposium on Superalloys-Superalloys 2008 Champion, Pennsylvania* **2008** 891
[9] Mottura A, Warnken M, Miller M K, Finnis M W and Reed R C 2010 *Acta Mater.* **58** 931
[10] Mottura A, Wu R T, Finnis M W and Reed R C 2008 *Acta Mater.* **56** 2669
[11] Mottura A, Finnis M W and Reed R C 2012 *Acta Mater.* **60** 2866
[12] Zhu T, Wang C Y and Gan Y 2010 *Acta Mater.* **58** 2045
[13] Huang M and Zhu J 2016 *Rare Met.* **35** 127
[14] Smith J 1987 *Effects of Cr and Re additions upon coarsening and deformation behavior of single-crystal Ni-base model superalloys* (Ph. D. Dissertation) (Illinois: Illinois University Urbana)
[15] Chen J Y, Feng Q, Cao L M and Sun Z Q 2011 *Mater. Sci. Eng. A* **528** 3791
[16] Ge B H, Luo Y S, Li J R and Zhu J 2010 *Scr. Mater.* **63** 969
[17] Huang M, Cheng Z Y, Xiong J C, Li J R, Hu J Q, Liu Z L and Zhu J 2014 *Acta Mater.* **76** 294
[18] Yu X X, Wang C Y, Zhang X N, Yan P and Zhang Z 2014 *J. Alloys Compd.* **582** 299
[19] Huang Y Y, Mao Z G, Noebe R D and Seidman D N 2016 *Acta Mater.* **121** 288
[20] Kresse G and Hafner J 1993 *Phys. Rev. B* **48** 13115
[21] Kresse G and Hafner J 1994 *Phys. Rev. B* **49** 14251
[22] Kresse G and Furthmüller J 1996 *Phys. Rev. B* **54** 11169
[23] Kresse G and Furthmüller J 1996 *Comput. Mater. Sci.* **6** 15
[24] Kresse G and Joubert D 1999 *Phys. Rev. B* **59** 1758
[25] Perdew J P, Burke K and Ernzerhof M 1996 *Phys. Rev. Lett.* **77** 3865
[26] Monkhorst H J and Pack J D 1976 *Phys. Rev. B* **13** 5188
[27] Methfessel M and Paxton A T 1989 *Phys. Rev. B* **40** 3616
[28] Luo Y S, Zhang L H, Wang Y M, Ge B H, Guo W, Zhan J, Zhang J X and Zhu J 2016 *Philos. Mag. Lett.* **96** 432
[29] Maisel S B, Schindzielorz N, Mottura A, Reed R C and Müller S 2014 *Phys. Rev. B* **90** 094110